

## Resonantly Enhanced Nonlinear Optical Probes of Oxidized Multiwalled Carbon Nanotubes at Supported Lipid Bilayers

Alicia C. McGeachy, Laura L. Olenick, Julianne M. Troiano, Ronald S. Lankone, Eric S Melby, Thomas R. Kuech, Eseohi Ehimighe, D. Howard Fairbrother, Joel A. Pedersen, and Franz M. Geiger

*J. Phys. Chem. B*, Just Accepted Manuscript • DOI: 10.1021/acs.jpcb.6b10141 • Publication Date (Web): 13 Jan 2017

Downloaded from <http://pubs.acs.org> on January 16, 2017

### Just Accepted

“Just Accepted” manuscripts have been peer-reviewed and accepted for publication. They are posted online prior to technical editing, formatting for publication and author proofing. The American Chemical Society provides “Just Accepted” as a free service to the research community to expedite the dissemination of scientific material as soon as possible after acceptance. “Just Accepted” manuscripts appear in full in PDF format accompanied by an HTML abstract. “Just Accepted” manuscripts have been fully peer reviewed, but should not be considered the official version of record. They are accessible to all readers and citable by the Digital Object Identifier (DOI®). “Just Accepted” is an optional service offered to authors. Therefore, the “Just Accepted” Web site may not include all articles that will be published in the journal. After a manuscript is technically edited and formatted, it will be removed from the “Just Accepted” Web site and published as an ASAP article. Note that technical editing may introduce minor changes to the manuscript text and/or graphics which could affect content, and all legal disclaimers and ethical guidelines that apply to the journal pertain. ACS cannot be held responsible for errors or consequences arising from the use of information contained in these “Just Accepted” manuscripts.



ACS Publications

The Journal of Physical Chemistry B is published by the American Chemical Society.

1155 Sixteenth Street N.W., Washington, DC 20036

Published by American Chemical Society. Copyright © American Chemical Society.

However, no copyright claim is made to original U.S. Government works, or works produced by employees of any Commonwealth realm Crown government in the course of their duties.

3  
4 ***Resonantly Enhanced Nonlinear Optical Probes of Oxidized Multiwalled Carbon***5  
6 ***Nanotubes at Supported Lipid Bilayers***7  
8 Alicia C. McGeachy,<sup>a</sup> Laura L. Olenick,<sup>a</sup> Julianne M. Troiano,<sup>a</sup> Ronald S. Lankone,<sup>b</sup> Eric  
9 S. Melby,<sup>c</sup> Thomas R. Kuech,<sup>c</sup> Eseohi Ehimiaghe,<sup>a</sup> D. Howard Fairbrother,<sup>b</sup> Joel A.  
10  
11 Pedersen,<sup>c,d</sup> Franz M. Geiger<sup>a,\*</sup>12  
13  
14  
15 <sup>a</sup>Department of Chemistry, Northwestern University, Evanston, IL 60208, <sup>b</sup>Department of  
16 Chemistry, Johns Hopkins University, Baltimore, Maryland 21218, <sup>c</sup>Environmental  
17  
18 Chemistry and Technology Program, University of Wisconsin, Madison, WI, 53706,  
19  
20  
2122 <sup>d</sup>Department of Chemistry, University of Wisconsin, Madison, WI, 53706, United States.  
23  
24  
25  
2627 \*Correspondence and requests for materials should be addressed to Franz Geiger  
28  
29 [geigerf@chem.northwestern.edu](mailto:geigerf@chem.northwestern.edu)  
30  
3132 **ABSTRACT**  
3334 With production of carbon nanotubes surpassing billions of tons per annum, concern  
35 about their potential interactions with biological systems is growing. Herein, we utilize  
36 second harmonic generation spectroscopy, sum frequency generation spectroscopy, and  
37 quartz crystal microbalance with dissipation monitoring to probe the interactions between  
38 oxidized multiwalled carbon nanotubes (O-MWCNTs) with supported lipid bilayers  
39 composed of phospholipids with phosphatidylcholine head groups as the dominant  
40 component. We quantify O-MWCNTs attachment to supported lipid bilayers under  
41 biogeochemically relevant conditions and discern that the interactions occur without  
42 disrupting the structural integrity of the lipid bilayers for the systems probed. The extent  
43  
44  
45  
46  
47  
48  
49  
50  
51  
52  
53  
54  
55  
56  
57  
58  
59  
60

1  
2  
3 of O-MWCNT sorption was far below a monolayer even at 100 mM NaCl and was  
4  
5 independent of the chemical composition of the supported lipid bilayer.  
6  
7  
8

## 9 10 I. INTRODUCTION. 11

12  
13 Carbon nanotubes (CNTs) have actual and proposed uses in application and consumer  
14 product areas including optics,<sup>1-2</sup> electronics,<sup>3-4</sup> biomedicine,<sup>5</sup> drug delivery,<sup>6-9</sup>  
15 environmental remediation<sup>10-14</sup> and energy technologies.<sup>15-16</sup> Applications and  
16 technologies that do not require specific chirality, diameters, or bandgaps often favor  
17 multiwalled CNTs (MWCNTs) over single walled carbon nanotubes because of the much  
18 lower cost and relative ease of productions of MWCNTs.<sup>17</sup> The projected increase in the  
19 use of CNT-based nanomaterials, however, raises concern about the potential adverse  
20 impacts new technologies utilizing these materials may have on the environment.<sup>18-26</sup>  
21  
22 Consequently, the possibilities of the environmental release of engineered nanomaterials  
23 in general,<sup>19, 27</sup> and MWCNTs in particular, and their subsequent interaction with  
24 biological systems have motivated laboratory studies of how they interact with  
25 biologically relevant systems of varying complexity,<sup>26, 28-29</sup> including idealized model  
26 systems consisting of phospholipid membranes.<sup>23, 30-35</sup> Several studies have indicated that  
27 CNTs may penetrate biological membranes, traverse the cell membrane, or may lead to  
28 alterations in cellular function, including death.<sup>36-43</sup>  
29  
30

31 Outside of the laboratory and in the environment, CNT surfaces are likely to contain  
32 oxygen-bearing functional groups.<sup>44-45</sup> Oxidized MWCNTs (O-MWCNTs) may thus  
33 represent a more realistic model system for studying the biogeochemical consequences of  
34 CNT release into the environment than pristine (unoxidized) CNTs.<sup>46-47</sup> Oxygen-  
35 containing functional groups are either grafted deliberately into the CNT sidewalls during  
36  
37  
38  
39  
40  
41  
42  
43  
44  
45  
46  
47  
48  
49  
50  
51  
52  
53  
54  
55  
56  
57  
58  
59  
60

1  
2  
3 covalent functionalization strategies or inadvertently as a result of exposure to oxidizing  
4 conditions.<sup>48-50</sup> The presence of oxygen-containing functional groups on CNTs increases  
5 their hydrophilicity<sup>51-52</sup> and stability in aqueous solutions.<sup>44, 53-55</sup> Although concentrations  
6 of O-MWCNTs in the environment have yet to be determined, current estimates based on  
7 a number of parameters including production rates suggest that CNT concentrations may  
8 be as high as several  $\mu\text{g}$  per kg of soil.<sup>56</sup> On the other hand, field experiments with natural  
9 benthic communities show that at least 2 mg of multiwalled CNTs per kg aquatic  
10 sediment were required to induce detectable changes in the structure of benthic organism  
11 communities.<sup>57</sup>

12  
13  
14  
15 Given the difficulty in determining the concentration of CNTs in environmental settings  
16 and the uncertainty in current estimates of environmental concentrations, determining O-  
17 MWCNT concentrations would be environmentally relevant in experimental laboratory  
18 model studies is challenging. Electrophysiological measurements conducted by Corredor  
19 *et al.* on suspended planar lipid bilayer membranes composed of 1,2-dioleoyl-*sn*-3-  
20 phosphatidylcholine (DOPC) suggest that O-MWCNTs at concentrations as low as 1.6  
21 mg/L can induce transmembrane current fluxes and possibly traverse the lipid bilayer.<sup>30</sup>  
22  
23 Yi and Chen explored the interactions between O-MWCNTs and DOPC under varying  
24 ionic strength and pH conditions using quartz crystal microbalance with dissipation  
25 monitoring (QCM-D). They reported no attachment of O-MWCNTs with surface oxygen  
26 concentrations of *ca.* 10% O to DOPC at 100 mM NaCl at pH 7.4 (10 mM HEPES) at O-  
27 MWCNT concentrations of 500  $\mu\text{g}/\text{L}$  as detected by QCM-D.<sup>33</sup> Though significant  
28 progress has been made in exploring the impact of CNTs on biological systems,  
29  
30  
31  
32  
33  
34  
35  
36  
37  
38  
39  
40  
41  
42  
43  
44  
45  
46  
47  
48  
49  
50  
51  
52  
53  
54  
55  
56  
57  
58  
59  
60

1  
2  
3 molecular-level insight into the interactions that occur between O-MWCNTs and  
4 biological systems remains limited.  
5  
6

7  
8 Here, we apply a multi-pronged approach to investigate the interactions of O-MWCNTs  
9 in the ng/L to mg/L concentration range with supported lipid bilayers (SLBs), which have  
10 been used as model systems for probing the interaction of O-MWCNT with cellular  
11 membranes.<sup>30, 34, 58-59</sup> We employ, for the first time, second harmonic generation (SHG)  
12 to track the adsorption of nanotubes to the SLB and estimate binding equilibria and  
13 adsorption free energies. We also report the first vibrational sum frequency generation  
14 (SFG) spectra of the carbon tail and headgroups within the lipids comprising the bilayer  
15 before, during, and after interaction with O-MWCNTs. Finally, we complement our  
16 spectroscopic measurements with mass measurements using QCM-D to estimate total  
17 mass attached. Our use of SLBs most likely prevents us from addressing possible  
18 experimental outcomes such as membrane piercing, and the formation of transmembrane  
19 channels, which molecular dynamics simulations<sup>34, 58-59</sup> and experiments<sup>30, 37</sup> indicate can  
20 occur under certain conditions. Instead, we focus on the initial step of attachment to the  
21 surface. We estimate the interaction free energies, and assess whether changes occur to  
22 the SLB structure before, during, and after interaction with the O-MWCNTs. Our results  
23 in the sub-ppb regime extend current molecular insights towards lower O-MWCNT  
24 concentrations than what had been available thus far, which may be of further relevance  
25 to biogeochemical conditions.  
26  
27

## 50 II. EXPERIMENTAL. 51

52 SHG and SFG spectroscopies are surface-general, label-free, and interface-specific  
53 techniques that allow interfacial processes to be monitored without the overwhelming  
54  
55  
56  
57  
58  
59  
60

1  
2  
3 contribution from bulk processes. When working with systems as complex as the nano-  
4 bio interface, we find that combining several techniques is advantageous in terms of  
5 facilitating data interpretation. Therefore, this work combines SHG and SFG  
6 spectroscopies, described below in section IIA-D, and QCM-D measurements, described  
7 below in section IIE.  
8  
9

10 **A. Laser System.** Detailed descriptions of our SHG approach can be found elsewhere.<sup>60</sup>  
11  
12

13 <sup>63</sup> In one set of experiments, an optical parametric amplifier (OPA-CF, Spectra-Physics)  
14 is tuned to a fundamental wavelength between 570-610 nm and a variable density filter is  
15 used to attenuate the energy of the 120 femtosecond pulses to  $0.40 \pm 0.05 \mu\text{J}/\text{pulse}$ ,  
16 translating to a pump fluence of approximately  $60 \text{ mJ}/\text{cm}^2$  to avoid thermal degradation  
17 of the sample and/or bilayer, as described in section III. The incident beam is focused to a  
18  $30 \mu\text{m}$  diameter focal spot, at an angle just below the angle of total internal reflection,  
19 onto a silica/water interface containing an SLB formed as described below. The reflected  
20 fundamental light is selectively filtered out through the use of appropriate optical filters  
21 and a monochromator tuned to the SHG wavelength. For reasons described below, a  
22 second set of experiments consisted of using the output from a 10 nJ, 120 femtosecond  
23 oscillator (Spectra Physics Mai Tai, 82 MHz) operating at 800 nm in lieu of the OPA  
24 output. In both sets of experiments, the second harmonic signal was collected using  
25 single photon counting methods as described elsewhere.<sup>60-63</sup> As described below, SHG  
26 bandwidth studies were conducted to confirm that fluorescence or similar sources of  
27 radiation other than SHG did not contribute to the observed SHG signal.  
28  
29

30 **B. Flow Cell, Substrate, Solution, and Bilayer Preparation.** The flow cell and bilayer  
31 preparation procedures used in our experiments has been described in detail before.<sup>63</sup> We  
32  
33

note that concerns about the potential “stickiness” or adhesion of O-MWCNTs to the PTFE tubing we use in our flow cell prompted us to increase the frequency with which we exchanged our tubing to once every other experiment. Before use, and between trials, the tubing was thoroughly rinsed with methanol, ultrapure water ( $\geq 18 \text{ M}\Omega\cdot\text{cm}$ ), and buffer solution. All other procedures used to prepare buffers and lipid bilayers were identical to those described earlier.<sup>63</sup> All buffers contained 10 mM Tris adjusted to pH 7.4 using dilute HCl or NaOH as needed and are henceforth referred to as Tris buffer.

For most of the work described herein, we studied SLBs formed from 1,2-dimyristoyl-3-*sn*-glycerophosphatidylcholine (DMPC), as phospholipids bearing zwitterionic PC headgroup are the majority lipids in extracellular leaflet of eukaryotic cell membranes.<sup>63</sup> To prepare vesicle suspensions, 2 mg of 1,2-dimyristoyl-*sn*-glycero-3-phosphocholine (DMPC, Avanti Polar Lipids) in chloroform were dried under a gentle stream of N<sub>2</sub>. The dried lipids were then placed in a vacuum desiccator overnight to remove any remaining organic solvent, and then stored in the freezer under nitrogen. Prior to use, the dried lipid vesicle films were rehydrated with a 100 mM NaCl, 10 mM Tris, 5 mM CaCl<sub>2</sub> solution at pH 7.4 and gently warmed to a temperature above the chain melting temperature ( $T_m = 24 \text{ }^\circ\text{C}$ )<sup>64</sup> for approximately 1 h. Vortexing the solution produced a suspension of multilamellar lipid vesicles that was then mechanically extruded through a polycarbonate membrane with a pore size of 0.05  $\mu\text{m}$  (Avanti Polar Lipids). The suspension was passed through the polycarbonate membrane 11 times, as suggested by the manufacturer. Bilayers composed of 1,2-dioleoyl-*sn*-glycero-3-phosphocholine (DOPC) and 1,2-dioleoyl-3-trimethylammonium-propane (DOTAP) were prepared in a similar fashion. The vesicle suspensions were stored in glass scintillation vials or polypropylene Falcon

tubes until use. Vesicle-containing suspensions were used within 2 d of preparation. The vesicle fusion method was employed to form supported lipid bilayers.<sup>65</sup> In SHG and SFG experiments, the flow cell was first equilibrated with Tris buffer containing 100 mM NaCl. After acquiring steady background signal, 4 mL of a 0.5 mg/mL vesicle-containing solution (100 mM NaCl, 10 mM Tris, 5 mM CaCl<sub>2</sub>, pH 7.4) were introduced into the flow cell. After allowing the SLB to form at the silica/water interface over the course of at least 20 minutes, the SLB was rinsed with CaCl<sub>2</sub>-free Tris buffer (100 mM NaCl) to remove remaining intact vesicles.

**C. Preparation and Characterization of O-MWCNT Suspensions.** A detailed procedure for the oxidation of MWCNTs is documented elsewhere.<sup>52, 46</sup> Briefly, pristine multiwall carbon nanotubes (MWCNTs) were purchased from NanoLab Inc. (Waltham, MA). The as-received MWCNTs were characterized by the manufacturer to have an outer diameter of 15 nm ± 5 nm, a length of 5-20 μm, and a carbon purity of > 95%. As described in detail in the Supporting Information, we used two different batches of oxidized MWCNTs that we prepared to contain 12% and 7% surface oxygen, denoted below as 7% and 12% O-MWCNTs, using H<sub>2</sub>SO<sub>4</sub>/HNO<sub>3</sub>. Uncertainties are in the 1% range. The CNT purification procedure developed by Bitter *et al.* (2014)<sup>46</sup> was followed for all O-MWCNTs produced. Transmission electron microscopy (TEM, Philips CM 300) was used to examine the structure of the O-MWCNTs following the oxidation procedure. TEM samples were prepared by dipping a lacey-carbon grid into a colloidal suspension of O-MWCNTs in water; the sample was imaged at 300 kV and the images were collected with a CCD camera (Figure 1A-B). Figure 1A shows that the oxidation process leaves the MWCNTs structurally intact with approximately 10 walls and lengths

1  
2  
3 on the order of several hundreds of nanometers. Dynamic light scattering (DLS) and laser  
4  
5 Doppler micro-electrophoresis (Zetasizer Nano ZS, Malvern Instruments, 632.8 nm, 173°  
6  
7 backscattering angle) were used to estimate changes in hydrodynamic diameter over time  
8  
9 and to measure electrophoretic mobility (EPM) for assessing the stability of aqueous O-  
10  
11 MWCNT-containing suspensions used in the SHG, SFG, and QCM-D experiments.  
12  
13

14  
15 **D. SHG Experiments.** In SHG adsorption experiments, the O-MWCNT-containing  
16 suspensions were introduced into the cell at a given nanotube concentration using a flow  
17 rate of 2.5 mL/min for a total volume of approximately 8 mL. To avoid changes in SHG  
18 signal that could be attributable to changes in ionic strength or pH, the O-MWCNT  
19 solutions were prepared such that the conditions of the background electrolyte and pH  
20 remained constant (1 or 100 mM NaCl, 10 mM Tris, pH 7.4). The pH of the particle  
21 suspensions was determined prior to each introduction and adjusted to pH 7.4 using dilute  
22 HCl and NaOH as necessary. Each suspension was vortexed for approximately 20 s  
23 immediately prior to introduction into the flow cell.  
24  
25  
26  
27  
28  
29  
30  
31  
32  
33  
34  
35

36  
37 **E. SFG Experiments.** Following our previously described approach,<sup>61,66</sup> we tune the  
38 broadband IR output of an OPA to the C–H stretching region between 2800 cm<sup>−1</sup> and  
39 3000 cm<sup>−1</sup>. SFG spectra are collected using near total internal reflection geometry and the  
40 ssp polarization combination, which probes components of the vibrational modes that are  
41 oriented perpendicular to the surface. Each SFG spectrum is composed of an average of  
42 five acquisitions each integrated over 4 min. In SFG experiments the SLBs were rinsed  
43 with 30 mL of Tris buffer at a flow rate of 1.5 mL/min because of the larger volume of  
44 the flow cell used in those experiments. SFG spectra of the SLBs before exposure to O-  
45  
46  
47  
48  
49  
50  
51  
52  
53  
54  
55  
56  
57  
58  
59  
60

1  
2  
3 MWCNTs (Figure 2) agree well with our previous report,<sup>63</sup> and are consistent with the  
4 presence of well-formed bilayers.  
5  
6

7  
8 **F. QCM-D Experiments.** QCM-D experiments were conducted using a modified version  
9 of our previously described procedures.<sup>63</sup> In these experiments, the particle attachment  
10 period was extended to 140 min, and the flow rate was reduced to 10  $\mu$ L/min. More  
11 details are provided in the Supporting Information.  
12  
13

### 14 III. RESULTS AND DISCUSSION

### 15

16  
17 **A. Assessing the Stability of O-MWCNT Suspensions.** Our DLS data indicate that  
18 some O-MWCNT aggregation occurs over the course of the SHG and SFG experiments(,  
19 while UV-Vis data indicate the absence of settleable aggregates (Figure 1C-D).  
20 Specifically, the UV-Vis data shown in Figure 1 indicates that the 7% O and 12% O  
21 MWCNTs are stable towards sedimentation over the timescale of the SHG and SFG  
22 experiments. Although DLS measurements (Figure 1E) indicate some aggregation of the  
23 O-MWCNTs occurs over the time period of the optical experiments (two hours), the  
24 increase in the hydrodynamic diameter ( $D_h$ ) of the 7% O-MWCNTs and 12% O-  
25 MWCNTs stabilizes after approximately 20 minutes at which point our SHG  
26 measurements are conducted. Comparable EPM values ( $-6.1 (\pm 2.9) \times 10^{-9} \text{ m}^2 \cdot \text{V}^{-1} \cdot \text{s}^{-1}$  and  
27  $-5.7 (\pm 1.1) \times 10^{-9} \text{ m}^2 \cdot \text{V}^{-1} \cdot \text{s}^{-1}$  for O-MWCNTs with surface oxygen concentrations of 7%  
28 and 12% O respectively) were obtained despite the difference in the relative percentage  
29 of oxygen-containing functional groups. The lack of correlation between the atomic  
30 percent surface oxygen concentration and the measured electrophoretic mobilities at pH  
31 values higher than 6 has been observed in other studies of O-MWCNTs.<sup>54</sup> These various  
32 particle stability measurements indicated that the SHG and SFG data are best described  
33  
34

1  
2  
3 as representing the interactions of individual O-MWCNTs and small O-MWCNT  
4 aggregates with SLBs.  
5  
6

7  
8 **B. Attachment of O-MWCNTs to Supported Lipid Bilayers Prepared from DMPC.**  
9

10 We recently determined that after accounting for the interfacial potential contributed by  
11 the SiO<sub>2</sub> substrate, SLBs rich in phospholipids with PC headgroups carry a negative  
12 interfacial potential at 100 mM NaCl at pH 7.4,<sup>63</sup> which is important, given the negative  
13 surface potentials of the O-MWCNTs used here. Upon exposure to 1 mg/L O-MWCNTs  
14 in the presence of 100 mM NaCl buffer, we observe a *ca.* 200 cm<sup>-1</sup> broad contribution  
15 underneath the relatively sharp vibrational features observed prior to O-MWCNT  
16 exposure for 7% O-MWCNTs (Figure 2A) and 12% O-MWCNTs (Figure 2B). We  
17 putatively attribute this broad spectral feature to the production of a non-resonant SFG  
18 response from the pool of polarizable free electrons associated with the  $\pi$ -electron system  
19 of the O-MWCNTs, reminiscent of the well-known nonresonant SFG response from  
20 polarizable metals.<sup>67</sup> Upon rinsing the bilayer with O-MWCNT-free solution, the SHG  
21 signal remains unchanged, indicating irreversible adsorption of O-MWCNTs to the SLBs  
22 over the timescale investigated.  
23  
24

25 The appearance of a non-resonant response, on top of which ride well-resolved  
26 vibrational features of the SLB, is observed in the majority of the experiments conducted  
27 across all three O-MWCNT samples. Yet, we note that a subset of experiments conducted  
28 with 7% O-MWCNTs produced no change in the SFG signal (i.e., no increased non-  
29 resonant background develops, see Supporting Information Figure S7), which we  
30 attribute to possible variation in aggregation state or solution stability for the batch used  
31  
32  
33  
34  
35  
36  
37  
38  
39  
40  
41  
42  
43  
44  
45  
46  
47  
48  
49  
50  
51  
52  
53  
54  
55  
56  
57  
58  
59  
60

1  
2  
3 in those specific experiments though these differences were not evident in UV-Vis and  
4  
5 DLS measurements.  
6  
7

8 QCM-D studies conducted under conditions similar to those discussed in the SFG  
9 experiments (100 mM NaCl buffer and 1 mg/L 7% O-MWCNTs) reveal a small but  
10 measurable frequency shift,  $\Delta f = -0.57 \pm 0.16$  Hz (Figure S5). Upon rinsing the SLB  
11 formed from DMPC with buffer solution (i.e., no O-MWCNT present), the frequency  
12 shift increases to  $-0.33 \pm 0.10$  Hz (Figure 3). This observation is attributable to the  
13 removal of weakly bound carbon nanotubes, some portion of the bilayer, or both, along  
14 with loss of associated water and electrolyte. However, given that the SFG results do not  
15 indicate further bilayer alteration (Figure 2), the rinsing likely leads to the loss of weakly  
16 bound 7% O-MWCNTs. QCM-D studies conducted under the same conditions with 12%  
17 O-MWCNTs yield larger frequency shifts of  $-3.5 \pm 1.7$  Hz, albeit with larger  
18 uncertainties of the point estimate (Figure 3) and no reversibility. The energy dissipation  
19 relative to the frequency changes for these systems ( $\Delta D_5/(\Delta f_5/5) = 9.4 (\pm 2.7) \times 10^{-7}$  Hz<sup>-1</sup>  
20 and  $8.3 (\pm 2.0) \times 10^{-7}$  Hz<sup>-1</sup> for the 7% and 12% O-MWCNTs, respectively) precludes  
21 application of the Sauerbrey equation to estimate the mass of O-MWCNTs on the  
22 SLBs.<sup>68</sup> Nevertheless, the small frequency shifts observed indicates that the surface  
23 coverages here are far below a monolayer.  
24  
25

26 **C. SHG Control Studies.** Given that these experiments are the first to employ SHG to  
27 probe O-MWCNTs at liquid/solid interfaces, we briefly discuss outcomes from the  
28 control experiments we carried out to assess the validity and origin of the detected  
29 nonlinear optical signals. When compared to the bare SLB response at 100 mM NaCl and  
30 10 mM Tris buffer (no O-MWCNTs present), we observed fractional SHG signal  
31  
32  
33  
34  
35  
36  
37  
38  
39  
40  
41  
42  
43  
44  
45  
46  
47  
48  
49  
50  
51  
52  
53  
54  
55  
56  
57  
58  
59  
60

1  
2  
3 intensity increases as large as approximately 20% at  $\lambda_{\text{SHG}} = 300$  nm (kHz amplifier laser  
4 source) for all of the O-MWCNTs studied. Adsorption of O-MWCNTs to bare silica or  
5 defects in the SLB structure cannot be ruled out as a potential source for the observed  
6 SHG signal increases, given that adsorption isotherms for bare silica yield similar  
7 fractional increases in SHG intensity though adsorption to the underlying silica support is  
8 unlikely given that micron-scale defects in the SLB structure have not been observed.  
9 Based on QCM-D frequency shifts (24-26 Hz) and surface coverages ( $\sim 3.4$  to  $4.1 \times 10^{14}$   
10  $\text{cm}^{-2}$ ), SFG spectroscopy (well-resolved spectra), AFM and fluorescence microscopy  
11 (diffusion coefficients of  $\sim 2 \mu\text{m}^2/\text{s}$ ) the method of forming supported lipid bilayers via  
12 the vesicle fusion method does result in the formation of fluid nearly complete supported  
13 lipid bilayers as was shown in our previously published work.<sup>63</sup> Given the QCM-D  
14 results indicating mass uptake upon introducing O-MWCNTs with surface oxygen  
15 concentrations of 7% and 12% to SLBs formed from DMPC, we interpret this SHG  
16 response to indicate nanotube attachment to the bilayer. Further, attachment of 7% O-  
17 MWCNTs to SLBs formed from DMPC, depends on ionic strength with no significant  
18 change in SHG signal intensity relative to the initial SLB is observed at 1 mM NaCl  
19 (Figure S6), indicative of a repulsive electrostatic interaction between the O-MWCNTs  
20 and the SLBs. Similar trends in the adsorption of O-MWCNT under conditions of  
21 increasing ionic strength were also described in other work investigating the interactions  
22 of O-MWCNT and SLBs formed from DOPC.<sup>33</sup> To be clear, the term attachment here  
23 should not be taken to imply that covalent bonds are formed. Instead, the expectation is  
24 that the O-MWCNTs are physically adsorbed to the SLBs.  
25  
26  
27  
28  
29  
30  
31  
32  
33  
34  
35  
36  
37  
38  
39  
40  
41  
42  
43  
44  
45  
46  
47  
48  
49  
50  
51  
52  
53  
54  
55  
56  
57  
58  
59  
60

To better understand the origin of our SHG signal gains, a second set of SHG experiments was conducted. At  $\lambda_{\text{SHG}} = 400$  nm (MHz oscillator laser source) we observe no change in SHG signal intensity upon interaction of SLBs formed from DMPC with O-MWCNTs (Figure 4). The finding of significant increases in the SHG response at 300 nm that coincide with O-MWCNT addition and a lack of signal increase at 400 nm indicates that SHG resonance enhancement, which can substantially boost signal intensities when the SHG wavelength matches an electronic transition in the surface-bound species,<sup>69-71</sup> may be an important contributor to the SHG signals recorded here. Indeed, given the optical absorbance features of the O-MWCNTs towards the shorter wavelengths (Figure 1), it is likely that our experiments are approaching electronic two-photon resonance with the  $\pi \rightarrow \pi^*$  transitions of the nanotubes. Yet, further experiments using SHG spectroscopy with varying incident and SHG wavelengths are needed to unambiguously assess the role of resonance enhancement here.

To determine the damage threshold of the SLB systems and the bare silica substrate in the presence of 2 mg/L O-MWCNT, we introduced, in two separate experiments, two concentrations (1 and 2 mg/L) of O-MWCNTs in 100 mM NaCl buffer to the flow cell and increased the incident visible pulse energy in increments of 0.05  $\mu\text{J}$  up to 0.5  $\mu\text{J}$ . Fits of a power function to the SHG intensity as a function of pulse energy yield a quadratic dependence at a concentration of 1 mg/L (Figure 5A) but deviate somewhat ( $P = 2.5$ ) at a concentration of 2 mg/L (Figure 5B). Departures from the expected quadratic dependence indicate optical breakdown, optical processes other than SHG, or sample damage, which may be attributable to nanotube aggregation specifically at the interface, as opposed to the bulk aqueous solution, and strong absorbance at this high concentration and pulse

1  
2  
3 energy. Given the data shown in Fig. 5A and 5B, all SHG experiments were carried out  
4 using nanotube concentrations  $\leq 1$  mg/L, and incident pulse energies of  $0.40 \pm 0.05$   $\mu$ J so  
5 as to remain within the regime of well-behaved SHG responses.  
6  
7

8 Additional SHG bandwidth studies show that SHG signals recorded at  $\lambda_{\text{SHG}}$  of 300 and  
9 400 nm (Figure 5C, 5D respectively) are well behaved, showing no evidence of  
10 fluorescence or radiation other than SHG entering the photomultiplier tube. Finally, SHG  
11 polarization studies carried out with *p*-polarized incident light and at  $\lambda_{\text{SHG}} = 300$  nm show  
12 that the SHG signal is well polarized along the surface normal (Figure 5E).  
13  
14

15 **D. SHG Adsorption Isotherm Measurements.** Having verified that the nonlinear signal  
16 response was indeed due to SHG, we proceeded to record the SHG response as a function  
17 of O-MWCNT (7% O) concentration. Figure 6 shows the average of 18 individual  
18 adsorption isotherm measurements, each time using a newly formed SLB and newly  
19 prepared O-MWCNT (7% O) suspension. We find that the SHG response increases with  
20 O-MWCNT (7% O) concentration and begins to plateau at approximately 10  $\mu$ g/L in the  
21 case of all O-MWCNTs investigated here, regardless of surface oxygen concentration.  
22 This plateau indicates some limiting surface coverage has been reached.  
23  
24

25 To provide an estimate for the interaction energy, we fit the Langmuir adsorption  
26 model<sup>72-74</sup> to the SHG adsorption isotherms. The Langmuir fit yielded an apparent  
27 equilibrium constant,  $K_{\text{L}}^{\text{app}}$ , of  $1.2 \pm 0.2$  L/ $\mu$ g and  $2.0 \pm 0.4$  L/ $\mu$ g for 100 mM NaCl buffer,  
28 corresponding to adsorption free energy estimates of  $-52 \pm 0.4$  kJ/mol<sub>C</sub> and  $-53 \pm 0.8$   
29 kJ/mol<sub>C</sub> for the O-MWCNTs with surface oxygen concentrations of 7% and 12%  
30 respectively. In this analysis, we used the 55.5 molar (or  $10^9$   $\mu$ g/L) concentration of water  
31 as a standard state for adsorption from solution.<sup>75</sup> Departures from the Langmuir model  
32  
33

1  
2  
3 could be attributable to the lack of reversibility, (direct or indirect) particle-particle  
4 interactions (e.g., O-MWCNT aggregation), and the heterogeneous nature of O-  
5 MWCNTs, and are likely to be masked by the uncertainty in the reported point estimate.  
6  
7  
8  
9

10 **E. O-MWCNT Adsorption to SLBs Prepared from DOPC and DOPC/DOTAP.** O-  
11 MWCNT with surface oxygen concentrations of 8% O also adsorbed to SLBs composed  
12 of zwitterionic DOPC and DOPC bilayers containing cationic 1,2-dioleoyl-3-  
13 trimethylammoniumpropane (DOTAP) (Figure 7). (The batch of O-MWCNTs used in  
14 these experiments had a surface oxygen concentration of 8%, while those described in the  
15 previous sections had 7% O.) While we hypothesized that the adsorption of these  
16 negatively charged O-MWCNT particles would be higher in the presence of DOTAP, a  
17 cationic lipid, our SHG signals were comparable across SLBs formed from DOPC,  
18 DMPC, and 9:1 DOPC/DOTAP (Figure 7). Given that the surface charge of the pure SLB  
19 formed from DOPC and 9:1 DOPC/DOTAP are comparable,<sup>63</sup> the lack of significant  
20 difference in the adsorption behavior for these two bilayer systems is not surprising.  
21  
22  
23  
24  
25  
26  
27  
28  
29  
30  
31  
32  
33  
34  
35  
36  
37  
38  
39  
40  
41  
42  
43  
44  
45  
46  
47  
48  
49  
50  
51  
52  
53  
54  
55  
56  
57  
58  
59  
60

#### IV. POSSIBLE INTERACTION MECHANISM AND CONCLUSIONS.

The results from our SHG, SFG and QCM-D studies show that O-MWCNTs attach to the SLB probed here at 100 mM NaCl to a small extent. Adsorption of the CNTs to the SLBs likely does not cause significant disruption or displacement of the SLB as indicated by the retention of the characteristic SFG spectral features associated with DMPC, despite the development of a strong non-resonant background. Yi and Chen<sup>33</sup> previously reported no attachment of O-MWCNTs (10.6% oxygen) to SLBs composed of DOPC below a NaCl concentration of 200 mM at pH 7.3 (0.2 mM NaHCO<sub>3</sub>) at 37 °C. The two studies differed with respect to lipids used to form SLBs (DOPC vs. DMPC), O-MWCNT

1  
2  
3 concentration, the nature and concentration of the buffer, flow rate, and, likely most  
4 importantly, temperature. Nonetheless, similar to the results of Yi and Chen,<sup>33</sup> we  
5 observe more attachment to SLBs formed from DMPC or DOPC at higher ionic strength  
6 and no attachment at lower ionic strength (1 mM NaCl).

7  
8 As the O-MWCNT carry small negative zeta potentials under the conditions of the  
9 experiments,<sup>33, 54-55</sup> and given that SLBs composed of lipids having zwitterionic  
10 headgroups carry negative interfacial potentials,<sup>56</sup> the mechanism by which O-MWCNTs  
11 adsorb to SLBs formed from DMPC and DOPC likely involves sizeable entropy gains as  
12 water molecules and electrolyte ions are displaced upon attachment of the nanotubes.  
13 Coulomb repulsion between the like-charged O-MWCNTs and the SLBs are thus  
14 overcome. Indeed, SHG experiments using bilayers prepared from 9:1 mixtures of  
15 DOPC/DOTAP, which are also associated with a negative interfacial potential under the  
16 experimental conditions,<sup>63</sup> yield comparable fractional increases in SHG intensity upon  
17 exposure to O-MWCNTs as that of DOPC and DMPC further supporting our conclusion.  
18  
19 In summary, we have employed SHG and SFG spectroscopy to directly probe O-  
20 MWCNTs interacting with supported lipid bilayers. We showed that O-MWCNT adsorb  
21 to SLBs rich in PC lipids at 100 mM NaCl under the conditions explored in this study  
22 and at concentration in the sub-nM range. Resonantly enhanced SHG spectroscopy  
23 served as a chemically specific probe and is demonstrated to provide higher sensitivity to  
24 sub- $\mu$ g/L O-MWCNT adsorption processes than QCM-D. We also showed that  
25 adsorption of O-MWCNTs to SLBs does not result in significant disruption or  
26 displacement of the lipid bilayer as indicated by SFG spectroscopy. We cannot, however,  
27 rule out the formation of pores or assess the extent of local disruption to the bilayer.  
28  
29  
30  
31  
32  
33  
34  
35  
36  
37  
38  
39  
40  
41  
42  
43  
44  
45  
46  
47  
48  
49  
50  
51  
52  
53  
54  
55  
56  
57  
58  
59  
60

## V. ACKNOWLEDGEMENTS

This work was supported by the National Science Foundation Center for Chemical Innovation Program, through the Center for Sustainable Nanotechnology under Grant No. CHE-1503408. ACM and JMT gratefully acknowledge support through the NSF Graduate Research Fellowship Program (GRFP). DLS and XPS work was performed in the Keck II facility of NUANCE Center at Northwestern University. The NUANCE Center is supported by NSEC (NSF EEC- 0647560), MRSEC (NSF DMR-1121262), the Keck Foundation, the State of Illinois and Northwestern University. We acknowledge Dr. Ken Livi and Anna Goodridge for TEM imaging.

**Supporting Information available.** Experimental details and control studies. SHG adsorption isotherms with SLBs formed from DOPC and 9:1 DOPC/DOTAP. SHG and SFG adsorption studies with SLBs formed from DMPC.

1  
2  
3  
4  
5  
6  
7  
8  
9  
10  
11  
12  
13  
14  
15  
16  
17  
18  
19  
20  
21  
22  
23  
24  
25  
26  
27  
28  
29  
30  
31  
32  
33  
34  
35  
36  
37  
38  
39  
40  
41  
42  
43  
44  
45  
46  
47  
48  
49  
50  
51  
52  
53  
54  
55  
56  
57  
58  
59  
60  
REFERENCES

(1) Shriyan, S. K.; Fontecchio, A. K., Analysis of Effects of Oxidized Multiwalled Carbon Nanotubes on Electro-Optic Polymer/Liquid Crystal Thin Film Gratings. *Opt. Express* **2010**, *18*, 24842-24852.

(2) Taib, N. A. M.; Bidin, N.; Haris, H.; Adnan, N. N.; Ahmad, M. F. S.; Harun, S. W., Multi-Walled Carbon Nanotubes Saturable Absorber in Q-Switching Flashlamp Pumped Nd:YAG Laser. *Opt. Laser Technol.* **2016**, *79*, 193-197.

(3) Huang, Z. L.; Gao, M.; Yan, Z. C.; Pan, T. S.; Liao, F. Y.; Lin, Y., Flexible Infrared Detectors Based on P-N Junctions of Multi-Walled Carbon Nanotubes. *Nanoscale* **2016**, *8*, 9592-9599.

(4) Wang, D.; Li, H. Y.; Li, M. F.; Jiang, H. Q.; Xia, M.; Zhou, Z., Stretchable Conductive Polyurethane Elastomer in Situ Polymerized with Multi-Walled Carbon Nanotubes. *J. Mater. Chem. C C* **2013**, *1*, 2744-2749.

(5) Servant, A.; Jacobs, I.; Bussy, C.; Fabbro, C.; da Ros, T.; Pach, E.; Ballesteros, B.; Prato, M.; Nicolay, K.; Kostarelos, K., Gadolinium-Functionalised Multi-Walled Carbon Nanotubes as a T-1 Contrast Agent for MRI Cell Labelling and Tracking. *Carbon* **2016**, *97*, 126-133.

(6) Fedeli, S.; Brandi, A.; Venturini, L.; Chiarugi, P.; Giannoni, E.; Paoli, P.; Corti, D.; Giambastiani, G.; Tuci, G.; Cicchi, S., The "Click-on-Tube" Approach for the Production of Efficient Drug Carriers Based on Oxidized Multi-Walled Carbon Nanotubes. *J. Mater. Chem. C B* **2016**, *4*, 3823-3831.

(7) Mandal, B.; Das, D.; Rameshbabu, A. P.; Dhara, S.; Pal, S., A Biodegradable, Biocompatible Transdermal Device Derived from Carboxymethyl Cellulose and Multi-Walled Carbon Nanotubes for Sustained Release of Diclofenac Sodium. *RSC Adv.* **2016**, *6*, 19605-19611.

(8) Afshari, R.; Mazinani, S.; Abdouss, M., Nanohybrid Nanoparticles Based on Chitosan/Functionalized Carbon Nanotubes as Anti-HIV Nanocarrier. *Nano* **2015**, *10*, 12.

(9) Moradian, H.; Fasehee, H.; Keshvari, H.; Faghihi, S., Poly(Ethyleneimine) Functionalized Carbon Nanotubes as Efficient Nano-Vector for Transfecting Mesenchymal Stem Cells. *Colloids Surf., B* **2014**, *122*, 115-125.

(10) Mubarak, N. M.; Sahu, J. N.; Abdullah, E. C.; Jayakumar, N. S., Removal of Heavy Metals from Wastewater Using Carbon Nanotubes. *Sep. Purif. Rev.* **2014**, *43*, 311-338.

(11) Das, R.; Ali, M. E.; Abd Hamid, S. B.; Ramakrishna, S.; Chowdhury, Z. Z., Carbon Nanotube Membranes for Water Purification: A Bright Future in Water Desalination. *Desalination* **2014**, *336*, 97-109.

(12) Kim, S. H.; Umar, A.; Kumar, R.; Algarni, H.; Al-Assiri, M. S., Poly(Acrylic Acid)/Multi-Walled Carbon Nanotube Composites: Efficient Scaffold for Highly Sensitive 2-Nitrophenol Chemical Sensor. *Nanosci. Nanotechnol. Lett.* **2016**, *8*, 200-206.

(13) Sun, H. Q.; Kwan, C.; Suvorova, A.; Ang, H. M.; Tade, M. O.; Wang, S. B., Catalytic Oxidation of Organic Pollutants on Pristine and Surface Nitrogen-Modified Carbon Nanotubes with Sulfate Radicals. *Appl. Catal., B* **2014**, *154*, 134-141.

(14) Gu, H. B.; Rapole, S. B.; Huang, Y. D.; Cao, D. M.; Luo, Z. P.; Wei, S. Y.; Guo, Z. H., Synergistic Interactions between Multi-Walled Carbon Nanotubes and Toxic Hexavalent Chromium. *J. Mater. Chem. C A* **2013**, *1*, 2011-2021.

(15) Salunkhe, R. R.; Ahn, H.; Kim, J. H.; Yamauchi, Y., Rational Design of Coaxial Structured Carbon Nanotube-Manganese Oxide (CNT-MnO<sub>2</sub>) for Energy Storage Application. *Nanotechnology* **2015**, *26*, 7.

(16) De Nicola, F.; Salvato, M.; Cirillo, C.; Crivellari, M.; Boscardin, M.; Scarselli, M.; Nanni, F.; Cacciotti, I.; De Crescenzi, M.; Castrucci, P., Record Efficiency of Air-Stable Multi-Walled Carbon Nanotube/Silicon Solar Cells. *Carbon* **2016**, *101*, 226-234.

(17) De Volder, M. F. L.; Tawfick, S. H.; Baughman, R. H.; Hart, A. J., Carbon Nanotubes: Present and Future Commercial Applications. *Science* **2013**, *339*, 535-539.

(18) Peijnenburg, W. J. G. M., et al., A Review of the Properties and Processes Determining the Fate of Engineered Nanomaterials in the Aquatic Environment. *Crit. Rev. Environ. Sci. Technol.* **2015**, *45*, 2084-2134.

(19) Nel, A. E.; Madler, L.; Velegol, D.; Xia, T.; Hoek, E. M. V.; Somasundaran, P.; Klaessig, F.; Castranova, V.; Thompson, M., Understanding Biophysicochemical Interactions at the Nano-Bio Interface. *Nat. Mater.* **2009**, *8*, 543-557.

(20) Chen, C.; Li, Y.-F.; Qu, Y.; Chai, Z.; Zhao, Y., Advanced Nuclear Analytical and Related Techniques for the Growing Challenges in Nanotoxicology. *Chem. Soc. Rev.* **2013**, *42*, 8266-8303.

(21) Xiao, Y.; Wiesner, M. R., Characterization of Surface Hydrophobicity of Engineered Nanoparticles. *J. Hazard. Mater.* **2012**, *215*, 146-151.

(22) Pelaz, B.; Charron, G.; Pfeiffer, C.; Zhao, Y.; de la Fuente, J. M.; Liang, X.-J.; Parak, W. J.; del Pino, P., Interfacing Engineered Nanoparticles with Biological Systems: Anticipating Adverse Nano-Bio Interactions. *Small* **2013**, *9*, 1573-1584.

(23) Chen, K. L.; Bothun, G. D., Nanoparticles Meet Cell Membranes: Probing Nonspecific Interactions. Using Model Membranes. *Environ. Sci. Technol.* **2014**, *48*, 873-880.

(24) Hassellöv, M.; Readman, J.; Ranville, J.; Tiede, K., Nanoparticle Analysis and Characterization Methodologies in Environmental Risk Assessment of Engineered Nanoparticles. *Ecotoxicology* **2008**, *17*, 344-361.

(25) Yi, P.; Chen, K. L., Influence of Solution Chemistry on the Release of Multiwalled Carbon Nanotubes from Silica Surfaces. *Environ. Sci. Technol.* **2013**, *47*, 12211-12218.

(26) Sarma, S. J.; Bhattacharya, I.; Brar, S. K.; Tyagi, R. D.; Surampalli, R. Y., Carbon Nanotube-Bioaccumulation and Recent Advances in Environmental Monitoring. *Crit. Rev. Environ. Sci. Technol.* **2015**, *45*, 905-938.

(27) Murphy, C. J., et al., Biological Responses to Engineered Nanomaterials: Needs for the Next Decade. *ACS Cent. Sci.* **2015**, *1*, 117-123.

(28) Bussy, C.; Pinault, M.; Cambedouzou, J.; Landry, M. J.; Jegou, P.; Mayne-L'hermite, M.; Launois, P.; Boczkowski, J.; Lanone, S., Critical Role of Surface Chemical Modifications Induced by Length Shortening on Multi-Walled Carbon Nanotubes-Induced Toxicity. *Part. Fibre Toxicol.* **2012**, *9*, 15.

(29) Luan, B. Q.; Huynh, T.; Zhou, R. H., Complete Wetting of Graphene by Biological Lipids. *Nanoscale* **2016**, *8*, 5750-5754.

(30) Corredor, C.; Hou, W.-C.; Klein, S. A.; Moghadam, B. Y.; Goryll, M.; Doudrick, K.; Westerhoff, P.; Posner, J. D., Disruption of Model Cell Membranes by Carbon Nanotubes. *Carbon* **2013**, *60*, 67-75.

(31) Sanchez, V. C.; Jachak, A.; Hurt, R. H.; Kane, A. B., Biological Interactions of Graphene-Family Nanomaterials: An Interdisciplinary Review. *Chem. Res. Toxicol.* **2012**, *25*, 15-34.

(32) Carney, R. P.; Astier, Y.; Carney, T. M.; Voitchovsky, K.; Silva, P. H. J.; Stellacci, F., Electrical Method to Quantify Nanoparticle Interaction with Lipid Bilayers. *ACS Nano* **2013**, *7*, 932-942.

(33) Yi, P.; Chen, K. L., Interaction of Multiwalled Carbon Nanotubes with Supported Lipid Bilayers and Vesicles as Model Biological Membranes. *Environ. Sci. Technol.* **2013**, *47*, 5711-5719.

(34) Gangopomu, V. K.; Capaldi, F. M., Interactions of Carbon Nanotube with Lipid Bilayer Membranes. *J. Nanomater.* **2011**, *6*.

(35) Jimenez-Cruz, C. A.; Kang, S. G.; Zhou, R. H., Large Scale Molecular Simulations of Nanotoxicity. *Wiley Interdiscip. Rev.: Syst. Biol. Med.* **2014**, *6*, 265-279.

(36) Saria, R.; Mouchet, F.; Perrault, A.; Flahaut, E.; Laplanche, C.; Boutonnet, J. C.; Pinelli, E.; Gauthier, L., Short Term Exposure to Multi-Walled Carbon Nanotubes Induce Oxidative Stress and DNA Damage in Xenopus Laevis Tadpoles. *Ecotoxicol. Environ. Saf.* **2014**, *107*, 22-29.

(37) Mu, Q. X.; Broughton, D. L.; Yan, B., Endosomal Leakage and Nuclear Translocation of Multiwalled Carbon Nanotubes: Developing a Model for Cell Uptake. *Nano Lett.* **2009**, *9*, 4370-4375.

(38) Bottini, M.; Bruckner, S.; Nika, K.; Bottini, N.; Bellucci, S.; Magrini, A.; Bergamaschi, A.; Mustelin, T., Multi-Walled Carbon Nanotubes Induce T Lymphocyte Apoptosis. *Toxicol. Lett.* **2006**, *160*, 121-126.

(39) Cui, D. X.; Tian, F. R.; Ozkan, C. S.; Wang, M.; Gao, H. J., Effect of Single Wall Carbon Nanotubes on Human HEK 293 Cells. *Toxicol. Lett.* **2005**, *155*, 73-85.

(40) Monteiro-Riviere, N. A.; Nemanich, R. J.; Inman, A. O.; Wang, Y. Y. Y.; Riviere, J. E., Multi-Walled Carbon Nanotube Interactions with Human Epidermal Keratinocytes. *Toxicol. Lett.* **2005**, *155*, 377-384.

(41) Murr, L. E.; Garza, K. M.; Soto, K. F.; Carrasco, A.; Powell, T. G.; Ramirez, D. A.; Guerrero, P. A.; Lopez, D. A.; Venzor, J., 3rd, Cytotoxicity Assessment of Some Carbon Nanotubes and Related Carbon Nanoparticle Aggregates and the Implications for Anthropogenic Carbon Nanotube Aggregates in the Environment. *Int. J. Environ. Res. Public Health* **2005**, *2*, 31-42.

(42) Shi, X. H.; Kong, Y.; Gao, H. J., Coarse Grained Molecular Dynamics and Theoretical Studies of Carbon Nanotubes Entering Cell Membrane. *Acta Mech. Sin.* **2008**, *24*, 161-169.

(43) Pogodin, S.; Baulin, V. A., Can a Carbon Nanotube Pierce through a Phospholipid Bilayer? *ACS Nano* **2010**, *4*, 5293-5300.

(44) Bai, Y. C.; Wu, F. C.; Lin, D. H.; Xing, B. S., Aqueous Stabilization of Carbon Nanotubes: Effects of Surface Oxidization and Solution Chemistry. *Environ. Sci. Pollut. Res.* **2014**, *21*, 4358-4365.

(45) Fores-Cervantes, D. X.; Maes, H. M.; Schaffer, A.; Hollender, J.; Kohler, H. P. E., Slow Biotransformation of Carbon Nanotubes by Horseradish Peroxidase. *Environ. Sci. Technol.* **2014**, *48*, 4826-4834.

(46) Bitter, J. L.; Yang, J.; Milani, S. B.; Jafvert, C. T.; Fairbrother, D. H., Transformations of Oxidized Multiwalled Carbon Nanotubes Exposed to UVC (254 nm) Irradiation. *Environ. Sci.: Nano* **2014**, 324-337.

(47) Yang, J.; Bitter, J. L.; Smith, B. A.; Fairbrother, D. H.; Ball, W. P., Transport of Oxidized Multi-Walled Carbon Nanotubes through Silica Based Porous Media: Influences of Aquatic Chemistry, Surface Chemistry, and Natural Organic Matter. *Environ. Sci. Technol.* **2013**, 47, 14034-14043.

(48) Savage, T., et al., Photoinduced Oxidation of Carbon Nanotubes. *J. Phys.: Condens. Matter* **2003**, 15, 5915-5921.

(49) Rosca, I. D.; Watari, F.; Uo, M.; Akasaka, T., Oxidation of Multiwalled Carbon Nanotubes by Nitric Acid. *Carbon* **2005**, 43, 3124-3131.

(50) Wang, Y.; Iqbal, Z.; Mitra, S., Rapidly Functionalized, Water-Dispersed Carbon Nanotubes at High Concentration. *J. Am. Chem. Soc.* **2006**, 128, 95-99.

(51) Yi, P.; Chen, K. L., Influence of Surface Oxidation on the Aggregation and Deposition Kinetics of Multiwalled Carbon Nanotubes in Monovalent and Divalent Electrolytes. *Langmuir* **2011**, 27, 3588-3599.

(52) Wepasnick, K. A.; Smith, B. A.; Schrote, K. E.; Wilson, H. K.; Diegelmann, S. R.; Fairbrother, D. H., Surface and Structural Characterization of Multi-Walled Carbon Nanotubes Following Different Oxidative Treatments. *Carbon* **2011**, 49, 24-36.

(53) Zhang, Q.; Huang, J.-Q.; Qian, W.-Z.; Zhang, Y.-Y.; Wei, F., The Road for Nanomaterials Industry: A Review of Carbon Nanotube Production, Post-Treatment, and Bulk Applications for Composites and Energy Storage. *Small* **2013**, 9, 1237-1265.

(54) Smith, B.; Wepasnick, K.; Schrote, K. E.; Cho, H.-H.; Ball, W. P.; Fairbrother, D. H., Influence of Surface Oxides on the Colloidal Stability of Multi-Walled Carbon Nanotubes: A Structure-Property Relationship. *Langmuir* **2009**, 25, 9767-9776.

(55) Smith, B.; Wepasnick, K.; Schrote, K. E.; Bertele, A. H.; Ball, W. P.; O'Melia, C.; Fairbrother, D. H., Colloidal Properties of Aqueous Suspensions of Acid-Treated, Multi-Walled Carbon Nanotubes. *Environ. Sci. Technol.* **2009**, 43, 819-825.

(56) Sun, T. Y.; Bornhoft, N. A.; Hungerbuhler, K.; Nowack, B., Dynamic Probabilistic Modeling of Environmental Emissions of Engineered Nanomaterials. *Environ. Sci. Technol.* **2016**, 50, 4701-4711.

(57) Velzeboer, I.; Peeters, E.; Koelmans, A. A., Multiwalled Carbon Nanotubes at Environmentally Relevant Concentrations Affect the Composition of Benthic Communities. *Environ. Sci. Technol.* **2013**, 47, 7475-7482.

(58) Lelimousin, M.; Sansom, M. S. P., Membrane Perturbation by Carbon Nanotube Insertion: Pathways to Internalization. *Small* **2013**, 9, 3639-3646.

(59) Prylutska, S., et al., Comparative Study of Membranotropic Action of Single- and Multi-Walled Carbon Nanotubes. *J. Biosci. Bioeng.* **2013**, 115, 674-679.

(60) Saslow Gomez, S. A.; Jordan, D. S.; Troiano, J. M.; Geiger, F. M., Uranyl Adsorption at the Muscovite (Mica)/Water Interface Studied by Second Harmonic Generation. *Environ. Sci. Technol.* **2012**, 46, 11154-11161.

(61) Hayes, P. L.; Malin, J. N.; Konek, C. T.; Geiger, F. M., Interaction of Nitrate, Barium, Strontium and Cadmium Ions with Fused Quartz/Water Interfaces Studied by Second Harmonic Generation. *J. Phys. Chem. A* **2008**, 112, 660-668.

(62) Achtyl, J. L.; Vlassiouk, I. V.; Surwade, S. P.; Fulvio, P. F.; Dai, S.; Geiger, F. M., Interaction of Magnesium Ions with Pristine Single-Layer and Defected Graphene/Water

1  
2  
3 Interfaces Studied by Second Harmonic Generation. *J. Phys. Chem. B* **2014**, *118*, 7739-  
4 7749.  
5 (63) Troiano, J. M., et al., Direct Probes of 4 nm Diameter Gold Nanoparticles  
6 Interacting with Supported Lipid Bilayers. *J. Phys. Chem. C* **2015**, *119*, 534-546.  
7 (64) Marra, J.; Israelachvili, J., Direct Measurements of Forces between  
8 Phosphatidylcholine and Phosphatidylethanolamine Bilayers in Aqueous-Electrolyte  
9 Solutions. *Biochemistry* **1985**, *24*, 4608-4618.  
10 (65) Anderson, T. H.; Min, Y.; Weirich, K. L.; Zeng, H.; Fygenson, D.; Israelachvili, J.  
11 N., Formation of Supported Bilayers on Silica Substrates. *Langmuir* **2009**, *25*, 6997-7005.  
12 (66) Dogangun, M.; Hang, M. N.; Troiano, J. M.; McGeachy, A. C.; Melby, E. S.;  
13 Pedersen, J. A.; Hamers, R. J.; Geiger, F. M., Alteration of Membrane Compositional  
14 Asymmetry by  $\text{LiCoO}_2$  Nanosheets. *ACS Nano* **2015**, *9*, 8755-8765.  
15 (67) Covert, P. A.; Hore, D. K., Assessing the Gold Standard: The Complex  
16 Vibrational Nonlinear Susceptibility of Metals. *J. Phys. Chem. C* **2015**, *119*, 271-276.  
17 (68) Reviakine, I.; Johannsmann, D.; Richter, R. P., Hearing What You Cannot See  
18 and Visualizing What You Hear: Interpreting Quartz Crystal Microbalance Data from  
19 Solvated Interfaces. *Anal. Chem.* **2011**, *83*, 8838-8848.  
20 (69) Corn, R. M.; Higgins, D. A., Optical Second Harmonic Generation as a Probe of  
21 Surface Chemistry. *Chem. Rev.* **1994**, *94*, 107.  
22 (70) Geiger, F. M., Second Harmonic Generation, Sum Frequency Generation, and  $\chi^{(3)}$ :  
23 Dissecting Environmental Interfaces with a Nonlinear Optical Swiss Army Knife. *Annu.  
24 Rev. Phys. Chem.* **2009**, *60*, 61-83.  
25 (71) Eisenthal, K. B., Liquid Interfaces Probed by Second-Harmonic and Sum-  
26 Frequency Spectroscopy. *Chem. Rev.* **1996**, *96*, 1343-1360.  
27 (72) Langmuir, D., *Aqueous Environmental Chemistry*; Prentice Hall: Upper Saddle  
28 River, NJ 1997.  
29 (73) Masel, R. I., *Principles of Adsorption and Reaction on Solid Surfaces*; John Wiley  
30 & Sons: New York, 1996.  
31 (74) Somorjai, G. A., *Chemistry in Two Dimensions*; Cornell University Press: Ithaca,  
32 1981.  
33 (75) Adamson, A. W., *Physical Chemistry of Surfaces*, 5th ed.; John Wiley & Sons:  
34 New York, 1990.  
35  
36  
37  
38  
39  
40  
41  
42  
43  
44  
45  
46  
47  
48  
49  
50  
51  
52  
53  
54  
55  
56  
57  
58  
59  
60

**Figure Captions.**

**Figure 1.** (A) Low- and (B) high-magnification TEM images of O-MWCNTs prepared by refluxing in 70%  $\text{HNO}_3$ . (C, D) UV-Vis absorbance spectra of 1 mg/L of (C) O-MWCNT (7% O) and (D) O-MWCNT (12% O) in 100 mM NaCl, 10 mM Tris buffer, pH 7.4 over the span of 2 h. (E) Effective hydrodynamic diameter ( $D_h$ ) of O-MWCNT with surface oxygen concentrations of 7% O (filled black circle) and 12% (open circle) O MWCNT suspensions at 1 mg/L, 100 mM NaCl, 10 mM Tris buffer, pH 7.4 as a function of time.

**Figure 2.** *ssp*-Polarized SFG spectra of SLBs formed from DMPC before (green) and after interaction with 1 mg/L O-MWCNT (gray), and after rinsing with 100 mM NaCl buffer solution (blue) at 100 mM NaCl.

**Figure 3.** Attachment of O-MWCNTs (1 mg/L) to supported lipid bilayers formed from DMPC at 100 mM NaCl (10 mM Tris buffer, pH 7.4) as determined by QCM-D. Decreases in frequency correspond to increases in mass. Frequency data are reported for the 5<sup>th</sup> harmonic. Error bars represent one standard deviation ( $n = 3$ ). Full QCM-D traces are provided in the Supporting Information.

**Figure 4.** Fractional increase in SHG signal intensity as a function of O-MWCNT concentration, in mg/L, in the presence of supported lipid bilayers formed from DMPC at 100 mM NaCl 10 mM Tris buffer at pH 7.4 as monitored at 600 nm ( $\lambda_{\text{SHG}} = 300$  nm, filled circle) and 800 nm ( $\lambda_{\text{SHG}} = 400$  nm, open circle) incident wavelengths.

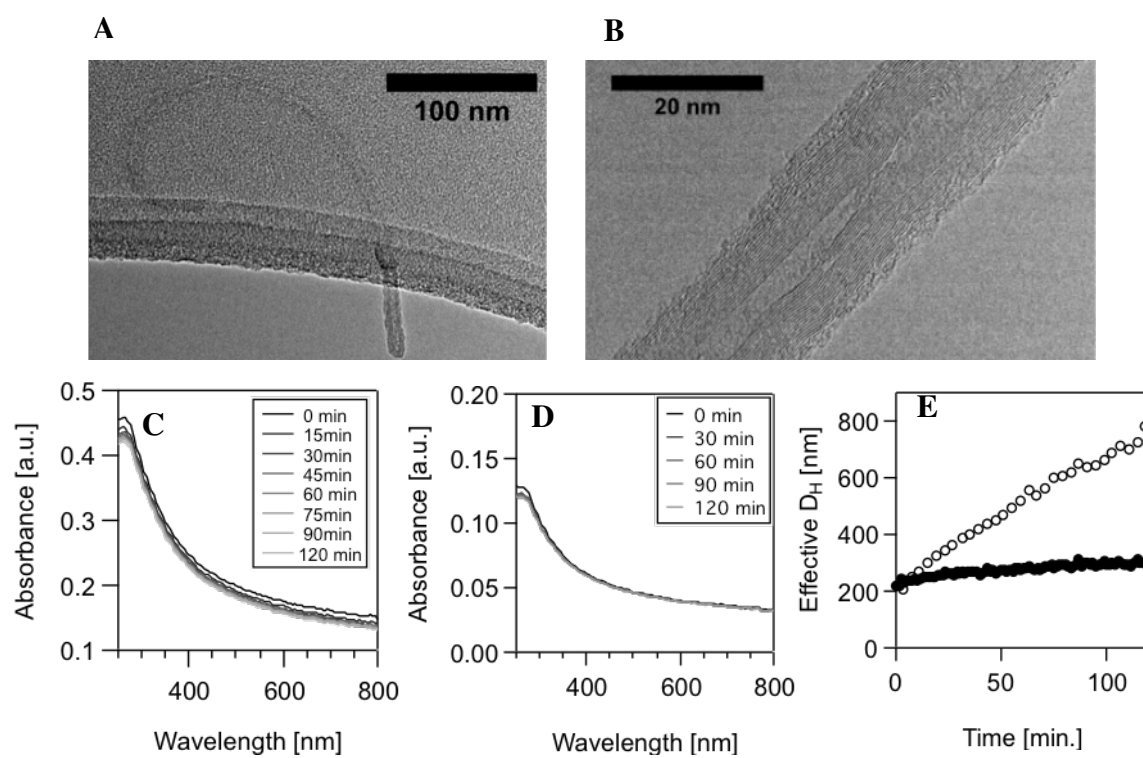
**Figure 5.** (A) Normalized SHG intensity as a function of pulse energy at 600 nm fundamental light field for 1 mg/L O-MWCNT interacting with an SLB formed from DMPC at 100 mM NaCl. Green curve is a power function of the form  $y = A + Bx^p$ , where

*p* = 2.1 ± 0.1. (B) Normalized SHG intensity as a function of pulse energy at 600 nm fundamental light field for 2 mg/L O-MWCNT interacting with an SLB formed from DMPC at 100 mM NaCl. The green curve is a power function of the form  $y = A + Bx^p$ , where  $p = 2.6 \pm 0.1$ . The black dashed line is a representative quadratic curve with a power of 2. (C) SHG intensity with the fundamental beam at 600 nm collected as a function of monochromator wavelength and Gaussian fit (solid green line) resulting in 3.9 ± 0.4 nm bandwidth for 2 mg/L concentration of O-MWCNT interacting with an SLB formed from DMPC at 100 mM NaCl, (D) SHG intensity with the fundamental beam at 800 nm collected as a function of monochromator wavelength and Gaussian fit (solid red line) resulting in 2.5 ± 0.1 nm bandwidth for 2 mg/L concentration of O-MWCNT interacting with an SLB formed from DMPC at 100 mM NaCl, (E) SHG intensity as a function of output polarization angle aligned with surface normal while probing with *p*-polarized fundamental light field for 2 mg/L O-MWCNT interacting with a SLB formed from DMPC at 100 mM NaCl.

**Figure 6.** SHG *E*-fields as a function of O-MWCNT concentration (7% O), in  $\mu\text{g}/\text{L}$ , collected at 300 nm, normalized to maximum *E*-field at high O-MWCNT concentration recorded at 100 mM NaCl, 25 °C, pH 7.4 in the presence of a SLB formed from DMPC at 100 mM NaCl and referenced to the SHG signal from an SLB formed from DMPC at the silica/water interface (filled circles). The black solid line is a fit of the Langmuir adsorption model to the experimental data collected at 100 mM NaCl in the presence of a SLB formed from DMPC, specifically of the form  $\theta = K_L^{\text{app}}C/(1+K_L^{\text{app}}C)$ , where  $K_L^{\text{app}}$  is the apparent equilibrium attachment constant, *C* is the concentration of O-MWCNT in

1  
2  
3       $\mu\text{g/L}$ , and  $\theta$  is the relative SHG E-field. Error bars are generated from the standard  
4  
5 deviation of data points collected at high particle concentration.  
6  
7

8      **Figure 7.** Fractional increase in SHG signal intensity as a function of O-MWCNT  
9 concentration, in  $\mu\text{g/L}$ , in the presence of supported lipid bilayers formed from 9:1  
10 DOPC/DOTAP (blue open circle), DOPC (red open circle), and DMPC (black open  
11 circle) at 100 mM NaCl 10 mM Tris buffer at pH 7.4. For both the DOPC and 9:1  
12 DOPC/DOTAP SLBs, the O-MWCNT used have surface oxygen concentrations of 8%  
13 while for the interaction studies involving DMPC, the concentration is 7% O.  
14  
15  
16  
17  
18  
19  
20  
21  
22  
23  
24  
25  
26  
27  
28  
29  
30  
31  
32  
33  
34  
35  
36  
37  
38  
39  
40  
41  
42  
43  
44  
45  
46  
47  
48  
49  
50  
51  
52  
53  
54  
55  
56  
57  
58  
59  
60



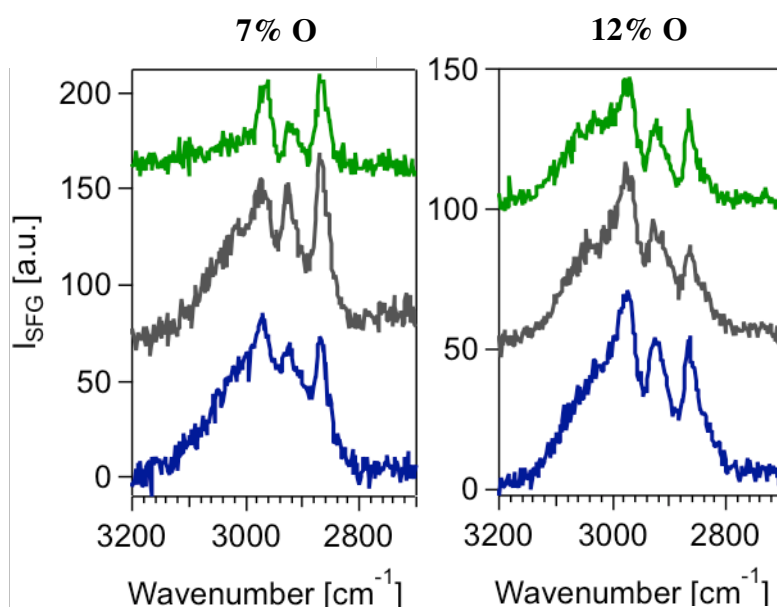


**Figure 2.**

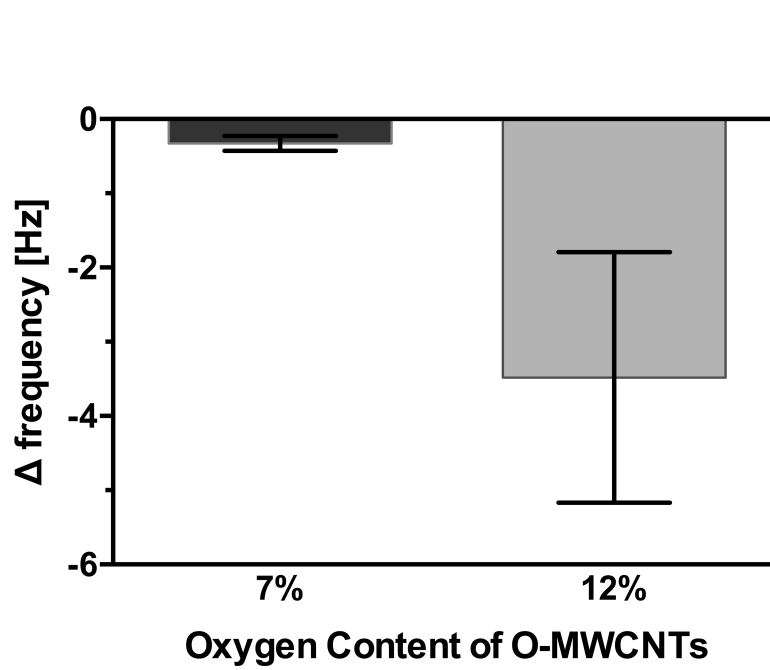


Figure 3.

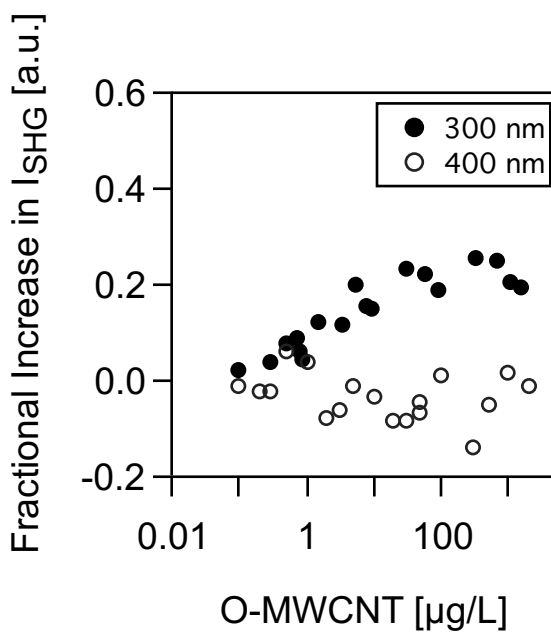


Figure 4.

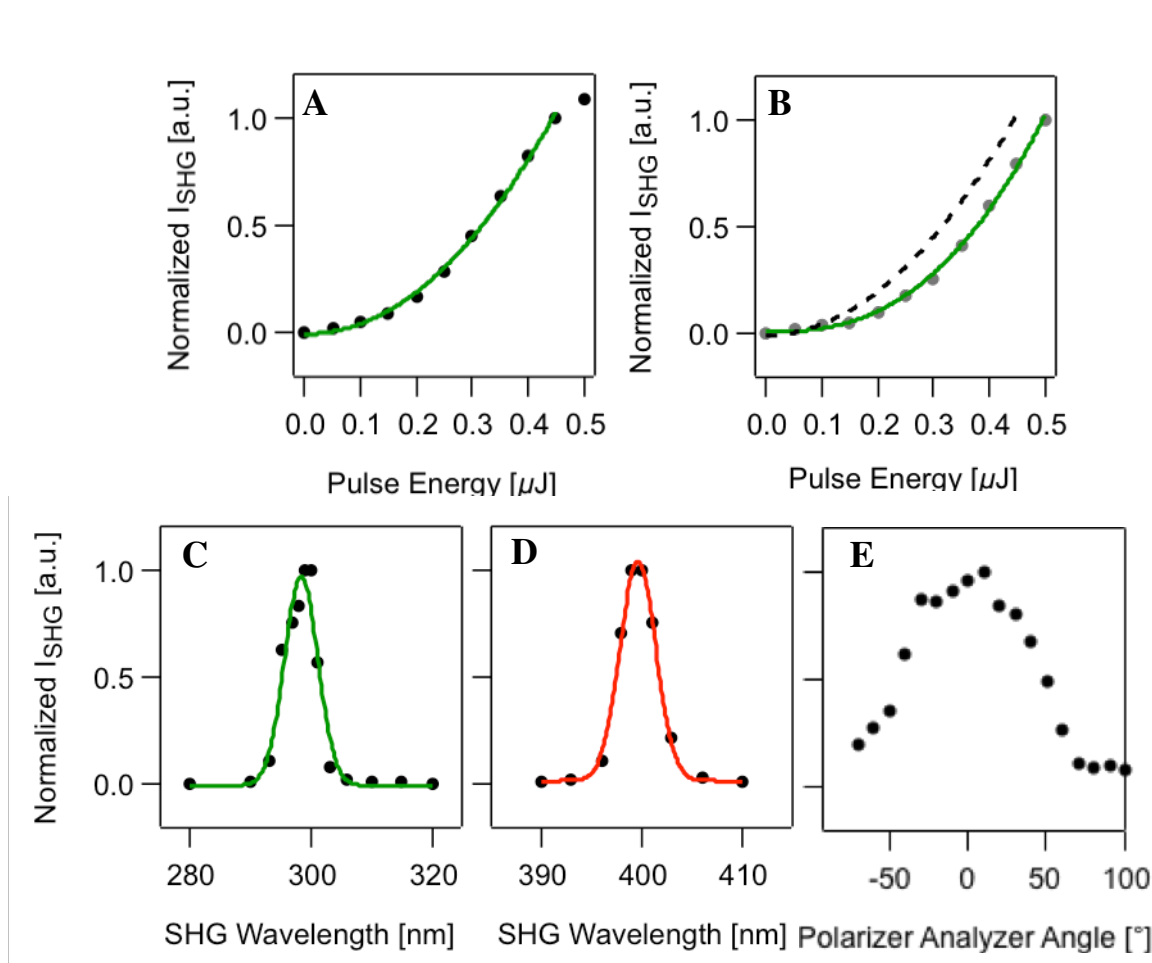
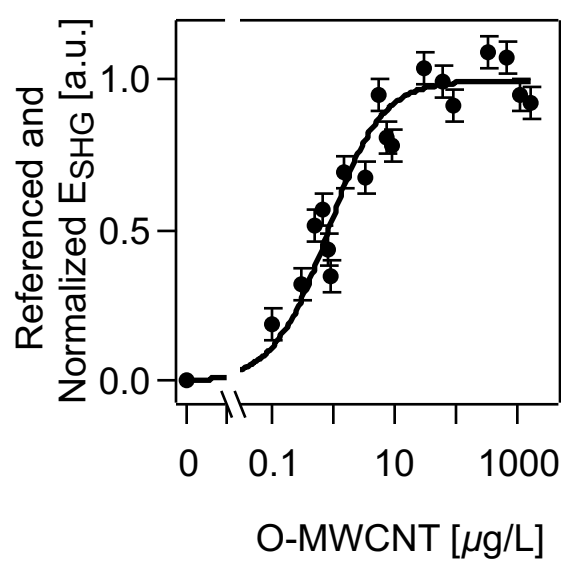
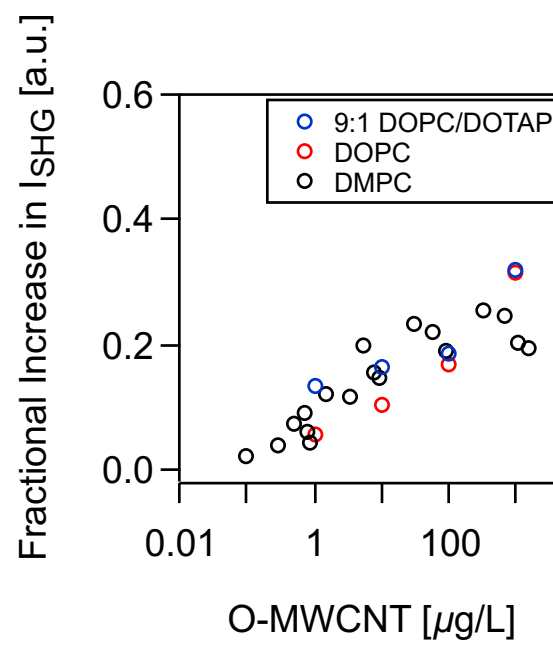


Figure 5.



**Figure 6.**



**Figure 7.**

1  
2  
3  
4  
5  
6  
7  
8  
9  
10  
11  
12  
13  
14  
15  
16  
17  
18  
19  
20  
21  
22  
23  
24  
25  
26  
27  
28  
29  
30  
31  
32  
33  
34  
35  
36  
37  
38  
39  
40  
41  
42  
43  
44  
45  
46  
47  
48  
49  
50  
51  
52  
53  
54  
55  
56  
57  
58  
59  
60

## TOC Graphic

